$KVPO_4F$ as a novel insertion-type anode for potassium ion batteries

Received 00th January 20xx,
Accepted 00th January 20xx

DOI: 10.1039/x0xx00000x

Hong Tan, Xiaoqiong Du, Jian-Qiu Huang, Biao Zhang *

$KVPO_4F$ is found to be capable of both accepting and donating K ions. As an anode, it delivers a reversible capacity of over 100 mAh/g with an average potential of 1.15 V vs K^+/K. The anode is also able to work under a wide temperature range of 0-55 °C.

Potassium ion batteries (PIBs) have emerged as promising alternatives to Li-ion batteries (LIBs) in some specific applications, such as stationary energy storage. The natural abundance of potassium element over lithium brings about the advantages of sustainability for up-coming PIBs. Moreover, the possibility of replacing copper by aluminum as a current collector on the anode side would further reduce the cost.[1] The major drawback of PIBs is the low energy density compared to LIBs at this stage. Although the battery chemistries utilizing alkali metal ions have similarities in many respects, the larger size of K ions than Li ions makes it difficult to design suitable host materials for both anode and cathode. Recently, some cathode materials such as Prussian-type $K_xMnFe(CN)_6$,[2] polyanionic $KVOPO_4$,[3] $K_3V_2(PO_4)_2F_3$,[4] and layered oxide[5,6] compounds have been synthesized with attractive energy densities. These achievements would greatly facilitate the development of PIBs with parallel progress on the anodes.

Various types of anodes have been explored, such as graphite,[7–9] hard carbon,[10,11] organic compounds,[12] and transitional metal chalcogenides.[13] Plenty of active sites have been discovered in the carbon-based anodes, enabling the tunable voltage profiles.[14] In the pursuit of high capacity, alloy-type anodes such as Bi and Sb have been explored.[15–18] Fabrication of nanostructure and construction of robust solid electrolyte interphase are conducted to alleviate the volume change and improve the cyclic stability.[19–21] The insertion-type anode is another important material that has been widely adopted in alkali-metal ion batteries, which is characteristic of excellent stability with suitable plateaus.[22] Considerable efforts have been put into the search of insertion-type anodes in PIBs. Several attractive candidates, including $K_2Ti_6O_{13}$[23] and MoS_2[24] have been reported with outstanding structural and cyclic stability, although the capacity is relatively low.

Herein we report a novel insertion-type anode $KVPO_4F$ that possesses a capacity of over 100 mAh/g with good stability. $KVPO_4F$ shares a similar structure with $KTiOPO_4$. It was firstly synthesized by Fedotov et al.[25] utilizing ion exchange method from $LiVPO_4F$. Following this, Komaba et al. chemically synthesized the phase and explored its performance as a cathode in PIBs, which exhibits a capacity of around 80 mAh/g at an average potential of 4.13 V vs. K^+/K.[3] The capacity could be further increased to 105 mAh/g through the preparation of stoichiometric $KVPO_4F$ as demonstrated by Ceder's group.[26] Despite the promising performance as a cathode, its behavior as an anode has never been studied. The K ions in $KVPO_4F$ are located at 4a site in the $Pna2_1$ space group. Careful examination of the structure reveals the K ion sites are not fully occupied, which implies that extra K ions could be accommodated. Moreover, the reduction of V^{3+} to V^{2+} in the polyanionic structure consisting of VPO_4 framework proves to be feasible as the case in $Na_3V_2(PO_4)_2F_3$.[27] Thus, we aim to explore the electrochemical performance of $KVPO_4F$ during K ion insertion when severing as an anode in PIBs.

$KVPO_4F$ is normally prepared by a two-step approach, where VPO_4 is produced firstly followed by reaction with KF.[3,26] A one-pot sol-gel method is used to synthesize the compound in this study, where KF, $NH_4H_2PO_4$, NH_4VO_3 are adopted as precursors. The well-mixed raw materials were calcinated at 700 °C for 8h under Ar atmosphere to obtain $KVPO_4F$. Detailed synthesis approach could be found in the supplemental information. The amount of KF is found to be critical in preparing the phase with high-purity. Our study suggests KF should be 20% in excess. With the stoichiometric amount of KF, the products tend to show poor crystallinity, and impurities such as $KVOPO_4$ was observed. We speculate part of KF is evaporated during the high-temperature calcination. More excess of KF to 50% would also deteriorate the structure as can be seen in Fig. S1. The XRD pattern of optimal $KVPO_4F$ phase is shown in Fig. 1a. Rietveld refinement using the structural model proposed by Fedotov et al.[25] indicates the compound is a pure phase that belongs to $Pna2_1$ space group. It has a lattice parameter of a=12.8289 Å, b=6.4046 Å, and c=10.6038 Å. The unit cell has a volume of 871.26 $Å^3$, which is slightly larger than $KVPO_4F$ obtained through the two-step approach.[3] The fluorine is prone to be substituted by oxygen during thermal annealing. The lattice parameters shown here are closer to the stoichiometric phase reported by Ceder G. et al,[26] indicating minimal oxygen doping on fluorine

Department of Applied Physics, the Hong Kong Polytechnic University, Hung Hom, Hong Kong, P.R. China;
Corresponding author: Biao Zhang. Email: biao.ap.zhang@polyu.edu.hk
† Footnotes relating to the title and/or authors should appear here.
Electronic Supplementary Information (ESI) available: [details of any supplementary information available should be included here]. See DOI: 10.1039/x0xx00000x

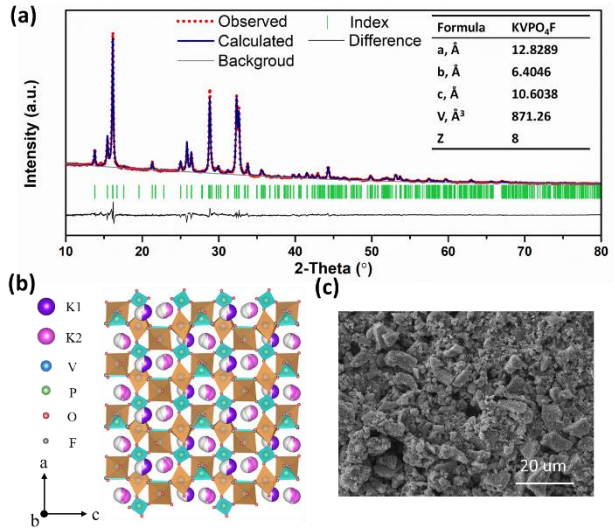

Fig. 1 (a) Rietveld refinement analysis of XRD pattern of the as-obtained $KVPO_4F$ and its lattice parameters; (b) crystal structure of $KVPO_4F$ displayed along b-axis; (c) SEM image of $KVPO_4F$.

site. Fig. 1b shows the refined structure, which consists of VO_4F_2 octahedra and PO_4 tetrahedra building blocks. Two K ion sites are identified and their precise positions are summarized in Table S1. Both sites are half occupied, indicating the possibility to accommodate one more K ion per $KVPO_4F$. Scanning electron microscopy (SEM, Fig. 1c) reveals the particles are agglomerated with a size ranging from around 2 to 20 µm. The primary particles have a size ranging from 50 to 100 nm, as demonstrated in transmission electron microscopy (TEM, Fig. S2).

Coin cells were assembled to evaluate the K ion insertion behavior in $KVPO_4F$ utilizing K metal as both the counter and reference electrode. 1 M KPF_6 in ethylene carbonate - propylene carbonate (EC-PC, 1:1 in volume) was used as the electrolyte. The working electrode is made of 70% $KVPO_4F$, 20% carbon SP conductive additive, and 10% Polyvinylidene fluoride binder. The voltage profiles of the first three cycles at a current of 100 mA/g are shown in Fig. 2a. It displays an initial discharge capacity of 295 mAh/g; while a charge capacity of only 150 mAh/g is observed, corresponding to a Coulombic efficiency of 51%. The large irreversible capacity arises mainly from the solid electrolyte interphase (SEI) formation. When carbon SP content is reduced to 5%, the initial irreversible capacity decreases from 145 mAh/g to 87 mAh/g (Fig. S3 a). A neat carbon SP electrode was further fabricated to demonstrate the speculation, where an extremely low Coulombic efficiency is found (Fig. S4). The Coulombic efficiency surges to 91% in the second cycle and a reversible capacity of 143 mAh/g is obtained, which is largely maintained in the following cycles. It is noted that part of the capacity is contributed by the conductive additives. Excluding the contribution, the $KVPO_4F$ anode delivers a capacity of 105 mAh/g. It indicates a reversible insertion/extraction of 0.8 K^+ per $KVPO_4F$.

To figure out the precise K ion insertion potential, the dQ/dV curves are plotted in Fig. 2b. Similar shapes and peak positions are observed for the first three cycles as a reflection of good reversibility of the K insertion and extraction process. The sharper peaks in the first cycle directly result from the flatter plateau in the initial discharge, but the positions are barely changed. Two reduction peaks locating at 1.0 and 0.8 V are observed in the discharge process, corresponding respectively to the two prominent peaks at 1.27 and 1.02 V upon oxidation. In-situ X-ray diffraction (XRD) tests were conducted to gain insights into the K ion insertion/extraction processes. A slurry consisting of active materials, conductive additives and binder were directly coated onto a beryllium current collector, which was also served as an X-ray transparent window in a Swagelok-type cell for in-situ XRD studies. The XRD patterns at various discharge states were recorded and presented in Fig. 2c. The discharge curves contain a plateau at 1.0 V followed by a sloping region. Once discharge to 1.0 V, a new peak at around 32 ° appears, while the original peaks, such as (411) and (221) that next to the position do not shift. The new peak progressively grows along with more K^+ insertion, accompanying with the decrease in peak intensity of (011) and (013). All the peak positions are barely changed, suggesting the formation of a new phase at this potential. In contrast, the newly formed peak gradually shifts to the lower angle during the sloping region, which indicates the expansion of the unit cell because of K ion intercalation in the solid-solution reaction. The original peaks at 17, 28.5, 32.5, 33.0 ° continuously diminish and a shoulder peak at 31 ° appears at 0 V. The precise atomic position cannot be accurately determined due to the low resolution of lab XRD with the interference of the beryllium window. Synchrotron XRD is ongoing to reveal the detailed phase transition. Upon charge, firstly the new peak at 31.4 ° moves back during the sloping region, followed by the reduction in the peak intensity at the plateau. Simultaneously, the peaks of $KVPO_4F$ emerge and fully recover at 3.0 V. The above observations demonstrate that a two-step process occurs during K^+ insertion, including a two-phase reaction at the 1.0 V plateau and a solid-solution reaction

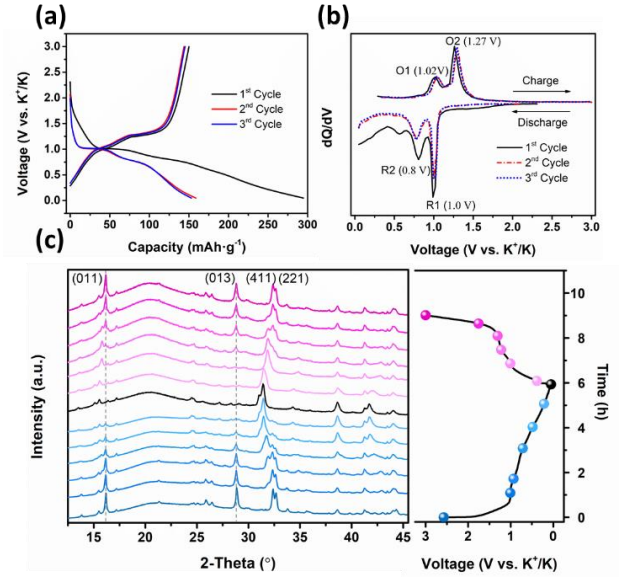

Fig. 2 (a) Voltage profiles of the 1st, 2nd and 3rd cycle for $KVPO_4F$ as anode at a current of 0.1 A/g; (b) dQ/dV curves derived from the voltage profiles in (a); (c) in-situ XRD patterns and the corresponding discharge - charge curve.

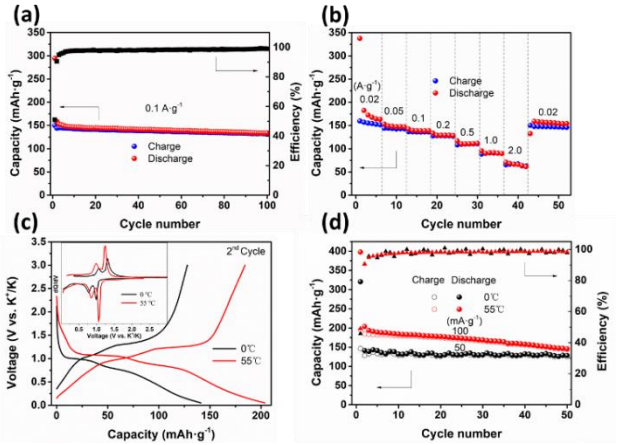

Fig. 3 (a) Cycling performance of $KVPO_4F$ as anode at 0.1 A/g; (b) Rate test of $KVPO_4F$ at 0.02, 0.05, 0.1, 0.2, 0.5, 1 and 2 A/g; (c) voltage profiles and (d) cyclic performance of $KVPO_4F$ at 0 ℃ and 55 ℃.

afterward in the sloping zone, both of which are reversible upon charge.

The long cyclic stability was examined at a current density of 0.1 A/g, as shown in Fig. 3a. A capacity of 133 mAh/g is retained after 100 cycles, accounting for 91% of its capacity in the 2nd cycle. The $KVPO_4F$ anode also possesses superb rate performance. Fig. 3b presents the capacities at increasingly current rates. It has a capacity of 153, 144, 137, 128, 110, 91, 65 mAh/g at a current density of 0.02, 0.05, 0.1, 0.2, 0.5, 1.0 and 2.0 A/g, respectively. Assuming a theoretical capacity of 131 mAh/g (corresponding to one K^+ per $KVPO_4F$), a current density 2.0 A/g equals to approximately 15 C. The good rate performance lies in the high K ion transfer coefficient of 1.3 and 2.9×10^{-10} cm^2/s upon discharge and charge as proved by GITT test (Fig. S5). The rate performance would be further improved with resorting to nanostructure. After cycling at such a high current rate, the capacity could be restored when the current is reduced back to 0.02 A/g. Comparing with other insertion-type anodes in PIBs, the performance obtained here is among the best (Table. S2). Furthermore, we also test the electrode with a higher content of active materials (90 wt.%) and electrode with a higher mass loading (4.0 mg/cm^2). The performance is largely maintained, as shown in Fig. S3 and Fig. S6.

The capability of working at a wide temperature range is crucial to rechargeable batteries. There are some concerns regarding the temperature behaviors of PIBs due to the large radius of K ions, which may be detrimental to its kinetics, especially at low temperatures. Previous studies indeed point out the poor performance of graphitic carbon anode at zero degree.[14] Thus, we examined the temperature behaviors of $KVPO_4F$. Fig. 3c presents the voltage profiles of the anode at 0 and 55 °C. They resemble the shape of that at room temperature, indicating the identical structural evolution during K ions insertion/extraction. The capacity is only slightly decreased to 128 mAh/g at 0 °C, which is maintained for 50 cycles, as shown in Fig. 3d. It suggests this novel anode is promising in low-temperature PIBs. Under a high temperature of 55 °C, the capacity climbs to 183 mAh/g at the 2nd cycle. Ruling out the Carbon SP's contribution, it delivers a capacity of 144 mAh/g, which is commensurate with the insertion of

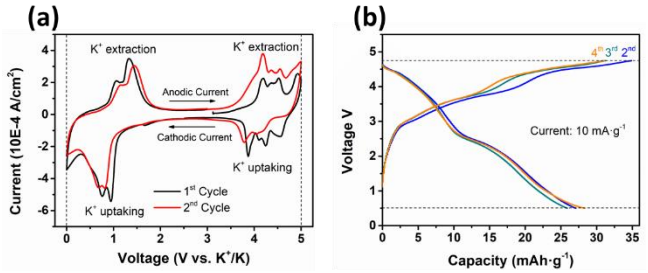

Fig. 4 (a) CV curves of $KVPO_4F$ half-cell within 0 - 5.0 V (vs. K^+/K); (b) voltage profiles of the 2nd-4th cycles for symmetric $KVPO_4F$ full-cell.

around one K ion to achieve a K_2VPO_4F phase. Nevertheless, a capacity degradation is observed when cycling at 55 °C, which may attribute to the damage of SEI at high temperature. This is confirmed by the negligible structural change of the $KVPO_4F$ and stabilization of the capacity after the cell is put back to 25 °C (Fig. S7). Building a robust SEI through electrolyte additive development in future studies would be beneficial to the stability at elevated temperatures.

Since $KVPO_4F$ is capable of both accepting and donating K ions, it enables us to assemble a symmetric cell utilizing $KVPO_4F$ as both anode and cathode. The cyclic voltammetry (CV) profiles scanning at a wide voltage of 0-5.0 V are plotted in Fig. 4a. It displays both V^{3+}/V^{4+} redox at a high potential of over 4.0 V and the V^{3+}/V^{2+} redox at a low potential of around 1.0 V. As a cathode, the $KVPO_4F$ delivers a capacity of 70 mAh/g between 3.0-4.95 V (Fig. S8). Coupling with a $KVPO_4F$ anode, a full cell was constructed. CV curves in the 2nd cycle show two reduction peaks at 4.5 and 2.5 V (Fig. S9), in agreement with the voltage profiles (Fig. 4b). An average discharge voltage of 2.5 V is obtained. Symmetric cell brings some advantages over the traditional battery, such as more resistible to volume change and reducing the fabrication cost.[28] The capacity of the full cell is not very attractive at this stage due to the low initial Coulombic efficiency (Fig. S10), arising from the large irreversible capacity of cathode and the SEI formation on the anode. Although the performance requires further optimization, the results presented here is the first prototype of symmetric PIBs to the best of our knowledge.

In summary, $KVPO_4F$ is explored as an anode for the first time. Up to one K ion could be reversibly inserted and extracted. In practical, a reversible capacity of 105 and 144 mAh/g has been achieved at 25 and 55 °C, respectively. It also shows a stable cyclic performance with a capacity retention of 91% after 100 cycles. Thanks to the high K ion diffusion coefficient, the $KVPO_4F$ delivers a reasonable capacity at a rate as high as 15C. The performance is largely maintained even at a low temperature of 0 °C, making it an attractive candidate for wide-temperature PIBs. Furthermore, this study enables the fabrication of symmetric cell utilizing $KVPO_4F$ as both an anode and cathode, which may bring advantages in cyclic life and cost.

B. Zhang gratefully acknowledges the financial support from the Hong Kong Research Grants Council through the Early Career Scheme (Project No. 25215918) and the Area of Excellence Project 1-ZE30 from the Hong Kong Polytechnic University. The authors are grateful to Dr. Xi Shen from the Hong Kong University of Science and Technology for the assistance on structural analysis.

Conflicts of interest

There are no conflicts to declare.

Notes and References

1 H. Kim, J. C. Kim, M. Bianchini, D. H. Seo, J. Rodriguez-Garcia and G. Ceder, *Adv. Energy Mater.*, 2018, **8**, 1702384.
2 X. Bie, K. Kubota, T. Hosaka, K. Chihara and S. Komaba, *J. Mater. Chem. A.*, 2017, **5**, 4325-4330.
3 K. Chihara, A. Katogi, K. Kubota and S. Komaba, *Chem. Commun.*, 2017, **53**, 5208-5211.
4 X. Lin, J. Huang, H. Tan, J. Huang and B. Zhang, *Energy Storage Mater.*, 2019, **16**, 97-101.
5 S. Guo, H. Zhang, K. Xi, K. Jiang, X. Zhang, Z. Liu and H. Zhou, *Chem. Commun.*, 2019, **55**, 7910-7913.
6 T. Masese, K. Yoshii, M. Kato, K. Kubota, Z. Huang, H. Senoh and M. Shikano, *Chem. Commun.*, 2019, **2**, 985-988.
7 J. Zhao, X. Zou, Y. Zhu, Y. Xu and C. Wang, *Adv. Funct. Mater.*, 2016, **26**, 8103-8110.
8 K. Share, A. P. Cohn, R. Carter, B. Rogers and C. L. Pint, *ACS Nano.*, 2016, **10**, 9738-9744.
9 J. Xu, Y. Dou, Z. Wei, J. Ma, Y. Deng, Y. Li, H. Liu and S. Dou, *Adv. Sci.*, 2017, **4**, 1700146.
10 Z. Jian, S. Hwang, Z. Li, A. S. Hernandez, X. Wang, Z. Xing, D. Su and X. Ji, *Adv. Funct. Mater.*, 2017, **27**, 1700324.
11 Z. Jian, Z. Xing, C. Bommier, Z. Li and X. Ji, *Adv. Energy Mater.*, 2016, **6**, 1501874.
12 C. Wang, W. Tang, Z. Yao and C. Fan, *Chem. Commun.*, 2019, **55**, 1801-1804.
13 J. Zhou, H. Zhao, Q. Zhang, T. Li, Y. Li, N. Lin and Y. Qian, *Chem. Commun.*, 2019, **55**, 1406-1409.
14 X. Lin, J. Huang and B. Zhang, *Carbon N. Y.*, 2019, **143**, 138-146.
15 W. Li, Y. Xu, Y. Dong, Y. Wu, C. Zhang, M. Zhou, Q. Fu, M. Wu and Y. Lei, *Chem. Commun.*, 2019, **55**, 6507-6510.
16 J. Huang, X. Lin, H. Tan and B. Zhang, *Adv. Energy Mater.*, 2018, **8**, 1703496.
17 Q. Zhang, J. Mao, W. K. Pang, T. Zheng, V. Sencadas and Y. Chen, *Adv. Energy Mater.*, 2018, **8**, 1703288.
18 Q. Liu, L. Fan, R. Ma, S. Chen, X. Yu, H. Yang, Y. Xie, X. Han and B. Lu, *Chem. Commun.*, 2018, **54**, 11773-11776.
19 K. Lei, C. Wang, L. Liu, Y. Luo, C. Mu and F. Li, *Angew. Chem. Int. Ed.*, 2018, **57**, 4687-4691.
20 J. Zheng, Y. Yang, X. Fan, G. Ji, X. Ji and C. Wang, *Energy Environ. Sci.*, 2019, **12**, 615-623.
21 J. Huang, X. Guo, X. Du, X. Lin, J. Huang, H. Tan, Y. Zhu and B. Zhang, *Energy Environ. Sci.*, 2019, **12**, 1550-1557.
22 V. Gabaudan, L. Monconduit, L. Stievano and R. Berthelot, *Front. Energy Res.*, 2019, **7**, 46.
23 S. Dong, Z. Li, Z. Xing, X. Wu, X. Ji and X. Zhang, *ACS Appl. Mater. Interfaces.*, 2018, **10**, 15542-15547.
24 X. Ren, Q. Zhao, W. D. McCulloch and Y. Wu, *Nano Res.*, 2017, **10**, 1313-1321.
25 S. S. Fedotov, N. R. Khasanova, A. S. Samarin, O. A. Drozhzhin, D. Batuk, O. M. Karakulina, J. Hadermann, A. M. Abakumov and E. V. Antipov, *Chem. Mater.*, 2016, **28**, 411-415.
26 H. Kim, D. Seo, M. Bianchini, R. J. Clément, H. Kim, J. C. Kim, Y. Tian, T. Shi, W. Yoon and G. Ceder, *Adv. Energy Mater.*, 2018, **8**, 1801591.
27 B. Zhang, R. Dugas, G. Rousse, P. Rozier, A. M. Abakumov and J.-M. Tarascon, *Nat. Commun.*, 2016, **7**, 10308.
28 S. Guo, H. Yu, P. Liu, Y. Ren, T. Zhang, M. Chen, M. Ishida and H. Zhou, *Energy Environ. Sci.*, 2015, **8**, 1237-1244.